Twisted scroll wave dynamics: Partially pinned waves in excitable chemical media

Journal:	*Physical Chemistry Chemical Physics*
Manuscript ID	CP-ART-11-2018-006948.R1
Article Type:	Paper
Date Submitted by the Author:	26-Dec-2018
Complete List of Authors:	Porjai, Porramain; Kasetsart Univiersity, Department of Physics Sutthiopad, Malee; Kasetsart Univiersity, Department of Physics Khaothong, Kritsana ; Kasetsart University, Department of Physics Phantu, Metinee ; Sa-nguang Ying School Kumchaiseemak, Nakorn ; Kasetsart University, Department of Physics Luengviriya, Jiraporn ; King Mongkut's University of Technology North Bangkok Showalter, Kenneth; West Virginia University, C. Eugene Bennett Department of Chemistry Luengviriya, Chaiya; Kasetsart University, Department of Physics

Twisted scroll wave dynamics: Partially pinned waves in excitable chemical media

Porramain Porjai, [a] Malee Sutthiopad, [b] Kritsana Khaothong, [b] Metinee Phantu,[c] Nakorn Kumchaiseemak, [b] Jiraporn Luengviriya,[d] Kenneth Showalter,[e,*] and Chaiya Luengviriya [b,*]

[a] *Division of Physics, Rajamangala University of Technology Thanyaburi, 39, Rangsit-Nakhonnayok Road, Thanyaburi, Pathum Thani , 12110, Thailand.*

[b] *Department of Physics, Kasetsart University, 50 Phaholyothin Road, Jatujak, Bangkok 10900, Thailand.*

[c] *Sa-nguang Ying School, 134 Prachatippatai Road, Amphur Muang, Suphanburi, 72000, Thailand.*

[d] *Lasers and Optics Research Center, Department of Industrial Physics and Medical Instrumentation, King Mongkut's University of Technology North Bangkok, 1518 Pibulsongkram Road, Bangkok 10800, Thailand.*

[e] *C. Eugene Bennett Department of Chemistry, West Virginia University, Morgantown, WV 26506-6045, USA.*

Corresponding authors:

*email: fscicyl@ku.ac.th

*email: kshowalt@wvu.edu

Abstract

We present an investigation of the dynamics of scroll waves that are partially pinned to inert cylindrical obstacles of varying lengths and diameters in three-dimensional Belousov-Zhabotinsky excitable media. Experiments are carried out in which a scroll wave is initiated with a special orientation to be partially pinned to the obstacle. Numerical simulations with the Oregonator model are also carried out, where the obstacle is placed in the region of the core of a preexisting freely rotating scroll wave. In both cases, the effect of the obstacle on the wave dynamics is almost immediately observable, such that after the first revolution of the wave, the pinned region of the scroll wave has a longer period than that of the freely rotating scroll wave. The dependence of the

scroll wave period on the obstacle position gives rise to a transition from a straight scroll wave to a twisted scroll wave in the pinned region, while the form of the freely rotating wave remains unchanged. The twisted scroll wave arises from the interaction of the freely rotating scroll wave with the obstacle, giving rise to a pinned twisted wave with the same period. The twisted scroll wave gradually advances, displacing the slower untwisted scroll wave until the scroll wave helically wraps around the entire obstacle. At this point, the period of the entire wave has a single value equal to that of the freely rotating scroll wave. The time for the transition to the twisted wave structure increases when either the obstacle length is increased or the obstacle diameter is decreased, while the average speed of the development increases with both the obstacle length and diameter. After the transition, the twisted wave remains stable, with its structure depending on the obstacle diameter – the larger the diameter, the shorter the helical pitch but the higher the twist rate.

I. INTRODUCTION

Spiral waves are self-organizing patterns that are typically observed in thin layers of excitable media [1]. In three-dimensional systems, their counterparts are scroll waves [2], which have more complicated dynamics. Each scroll wave rotates around a thin tube-like volume of continuous phase singularity called a filament, which can have various shapes, ranging from simple straight lines to highly complex forms [3].

Scroll waves are believed to play a role in cardiac arrhythmia and are therefore important to human health. Furthermore, severe maladies such as life-threatening cardiac fibrillation may occur if scroll waves become unstable and subsequently break into multiple uncoordinated segments, giving rise to a form of turbulence [4, 5]. Multiple mechanisms of spiral wave breakup have been identified in modeling studies of cardiac electrical activity [6]. Even for simple cases, such as straight scroll waves in homogeneous media, the linear filaments may elongate and become highly complex before their breakup takes place. This occurs when the medium excitability gives rise to the negative tension instability [7-11] or the 3D meandering instability [8, 11-13].

In media in which there is a gradient of excitability, the period of propagating scroll waves is position dependent. When the gradient is aligned with the scroll wave filament, a straight scroll wave becomes a twisted scroll wave. The straight filament deforms to a helical filament when the

twist rate reaches a threshold, which is termed a twist-induced instability [8, 14, 15]. The development of helical filaments has been realized in the excitable medium of the Belousov-Zhabotinsky (BZ) reaction with a gradient of temperature [16, 17], oxygen [18], or CO_2 [19, 20].

The propagation of spiral waves in the presence of obstacles has been of particular interest, as veins or scars might act as obstacles that pin spiral waves in cardiac tissues and potentially give rise to tachycardia [21]. In thin layers of excitable media, pinned spiral waves propagate with periods, wavelengths, and speeds larger than those of freely rotating spiral waves, and each of these measures increases with the obstacle circumference [22-26]. Furthermore, the increase of wave speed by an obstacle increases the difficulty of eliminating pinned spiral waves with a wave train [27, 28] or external forcing [29, 30].

In 3D systems, various effects of obstacles on the dynamics of scroll waves have been reported. The lifetime of a scroll ring is lengthened when its closed loop filament is partially pinned to an obstacle [31, 32]. A self-wrapping of a scroll ring results in the filament reshaping as well as elongating, i.e., the length of pinning to a cylindrical obstacle increases with time [33]. When a scroll wave is partially pinned to a slowly moving obstacle, the filament of the freely rotating part, whose end is attached to the system wall, is gradually stretched over the course of time [34]. Large cylindrical obstacles cause sudden changes in the front velocity of partially pinned scroll waves, which lead to wave breakups far from the filament and subsequently spatiotemporal chaos [35]. However, for media of low excitability, where wave turbulence usually occurs via the negative tension instability, thin cylindrical obstacles can suppress such turbulence and bring the waves into coordinated propagation [36].

In this paper, we present a study of the evolution of scroll waves partially pinned to cylindrical obstacles in the excitable BZ reaction. Unlike the cases of gradients of excitability, twisted waves are developed by the partial pinning, with their structure depending on the obstacle length and diameter. In addition, we have performed simulations using the Oregonator model [37, 38], which agree well with our experimental findings.

II. EXPERIMENTS

A. Experimental Methods

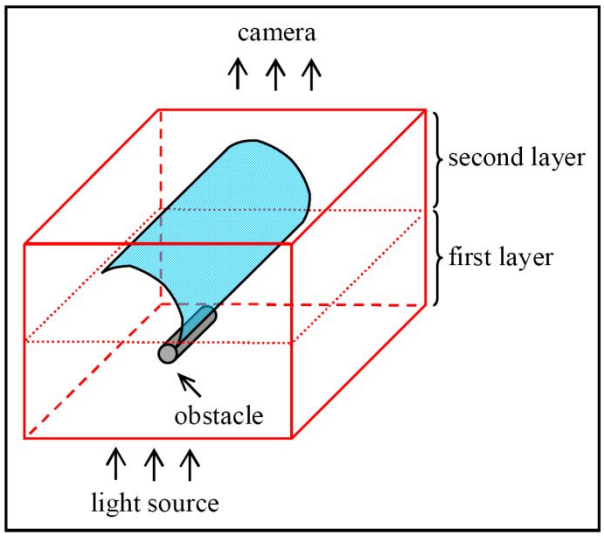

Fig. 1. Schematic representation of the experimental setup. A scroll wave partially pinned to an obstacle is initiated by using a two-layer method. The reactor is set between a white light source and a camera to record the top projection of the scroll wave.

The BZ reaction mixture is composed of 50.0 mM sodium bromate, 50.0 mM malonic acid, 140.0 mM sulfuric acid, and 0.625 mM ferroin (all from Merck). In addition, 50.0 mM sodium dodecyl sulfate (Fluka) and 1.0%wt/wt agarose gel (Sigma) are used to minimize bubble production and hydrodynamic perturbations, respectively. The gelled BZ medium is prepared as described in Ref. [39]. The dynamics of partially pinned scroll waves is studied using a transparent Plexiglas reactor with a volume of $30\times40\times10$ mm^3. Two series of cylindrical obstacles are used: (1) cylinders with a fixed diameter of 2.0 mm and different lengths of 5.0 mm to 25.0 mm, and (2) cylinders with a fixed length of 20.0 mm and different diameters of 1.0 mm to 2.0 mm. As shown in the schematic diagram in Fig. 1, the reactor is located between a white light source and a digital microscope camera, with a CMOS sensor size of 2 M pixels (Andonstar). Top projection images are recorded every 5.0 s, with a resolution of 20 μm pixel^{-1}, and stored in a computer via a USB port. During the experiments, the temperature of the laboratory is controlled at 24.0 ± 1.0 °C.

A partially pinned scroll wave is initiated by using a two-layer method, similar to the method described in Ref. [29]. A volume of the gel containing BZ solution is poured into the reactor to form the first layer, approximately 5 mm in thickness. The gelling temperature is about 26 °C. During the gelation, a cylindrical obstacle made from chemically inert plastic is embedded into the top part of the first layer. It is aligned to be parallel to the 30 mm side of the reaction vessel. Note that the obstacle is shorter than the length of the reaction vessel (see Fig. 1). A silver wire with a length of 30 mm is temporary immersed between the obstacle and the reactor wall to initiate two wave fronts. While one wave front moves towards the obstacle, the other front propagates to the wall and is subsequently annihilated. Another volume of the BZ solution at ~30 °C is quickly added on top of the first layer, and the wave front reaching the obstacle begins to curl in, forming a partially pinned scroll wave.

B. Experimental Results

Figure 2 illustrates the dynamics of the partially pinned scroll wave in the BZ medium. Unlike spiral waves in thin layers of BZ reaction mixture, which appear as sharp blue fronts on a red background (see, e.g. [29]), the original projection images of the scroll wave in the 10 mm thick medium are quite dark, and the image brightness and contrast are enhanced in order to improve the visualization. In these projection images, the lighter shades correspond to higher concentrations of the oxidized catalyst, ferriin. While the scroll wave in the upper region can rotate freely, the scroll wave in the lower region is pinned to the cylindrical obstacle. Shortly after the wave initiation is completed, the wave front that has just begun to curl has a simple form, with its projection appearing as a straight line close to the obstacle, as shown in Fig. 2(a). However, the difference in wave propagation in the upper and lower regions can be observed very early after the wave initiation. While the waves remain connected, the freely rotating wave moves ahead of the pinned wave after the first rotation, whose period is increased by the obstacle, Fig. 2(b).

Due to the difference in the wave period, the faster freely rotating scroll wave advances to displace the slower pinned scroll wave. However, a twisted wave structure develops from the interaction of the freely rotating wave with the obstacle such that the periods of the free and twisted waves are the same. During a transient time interval τ, during which the wave structure develops, the scroll wave consists of a twisted segment in the middle of two straight waves in the top and the bottom regions, Fig. 2(c). Once the faster pinned twisted scroll wave advances to completely

displace the slower pinned scroll wave, the medium is occupied by two wave structures: a freely rotating straight scroll wave and a twisted scroll wave that is helically wrapped around the obstacle, Fig. 2(d). This structure remains for several hours, as shown in Fig. 2(e), and it is observed in all experiments using obstacles of different lengths and diameters. Note that the freely rotating scroll wave remains almost straight during the experiments, which indicates that its filament is also straight, as shown by the dotted line in Fig. 2(e)

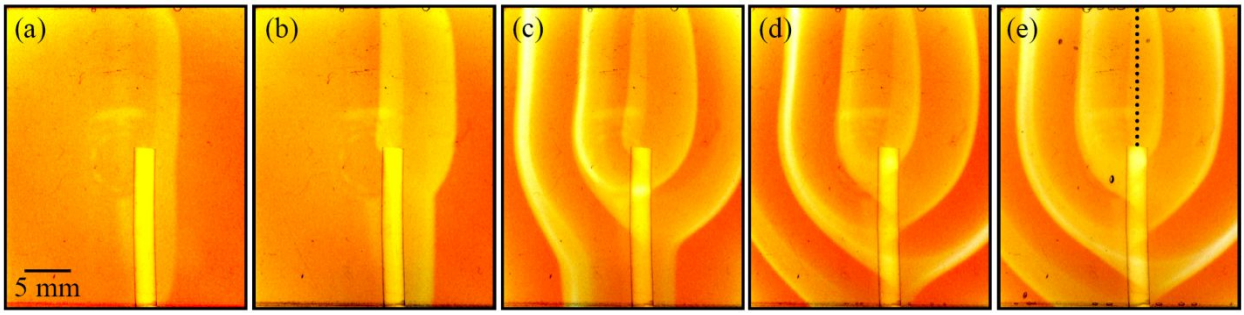

Fig. 2. Top Projection images of a partially pinned scroll wave in an excitable BZ medium: (a) 2.0 min, (b) 10.0 min, (c) 40.0 min, (d) 75.0 min, and (e) 130.0 min after the initiation of the scroll wave. The lower half of the scroll wave is pinned to a cylindrical obstacle of 2.0 mm in diameter and 15.0 mm in length. The dotted line in (e) indicates an estimate of the filament location of the freely rotating wave.

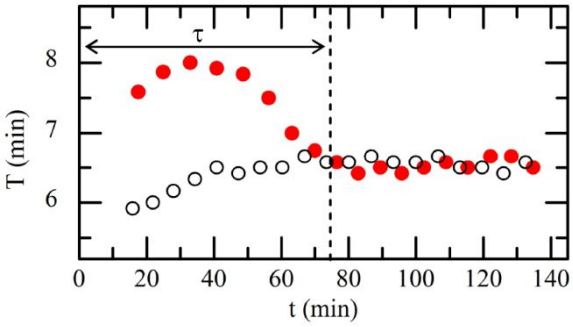

Fig. 3. Period *T* of partially pinned scroll wave shown in Fig. 2 as a function of time. Open (white) and filled (red) circles represent the period of the freely rotating scroll wave in the upper region and the pinned scroll wave in the lower region, respectively. The periods were measured at the top and bottom of the recorded projection images, such as those shown in Fig. 2. The cylindrical obstacle dimensions are 2.0 mm in diameter and 15.0 mm in length. The period of both the unpinned and pinned scroll waves become equal after a transient time interval τ.

Figure 3 shows an example of the wave periods of the partially pinned scroll wave as a function of time. The periods are measured from the projection images (e.g., as shown in Fig. 2). They are defined as the time delays between consecutive wave fronts arriving at the measuring positions. The periods of the freely rotating wave and the pinned part are measured at the top and bottom of the images, respectively. During the first 30 to 40 minutes, the periods of both the unpinned and pinned scroll waves increase as the gelled BZ medium cools from ~30 °C to the controlled room temperature of 24.0 °C. Note that the gelling temperature is about 26 °C. The period of the unpinned wave becomes approximately constant for $t > 40$ min; however, the period of the pinned wave decreases, and within 5 wave rotations the periods of both the pinned and unpinned waves become very similar, as the pinned twisted scroll wave displaces the original pinned scroll wave.

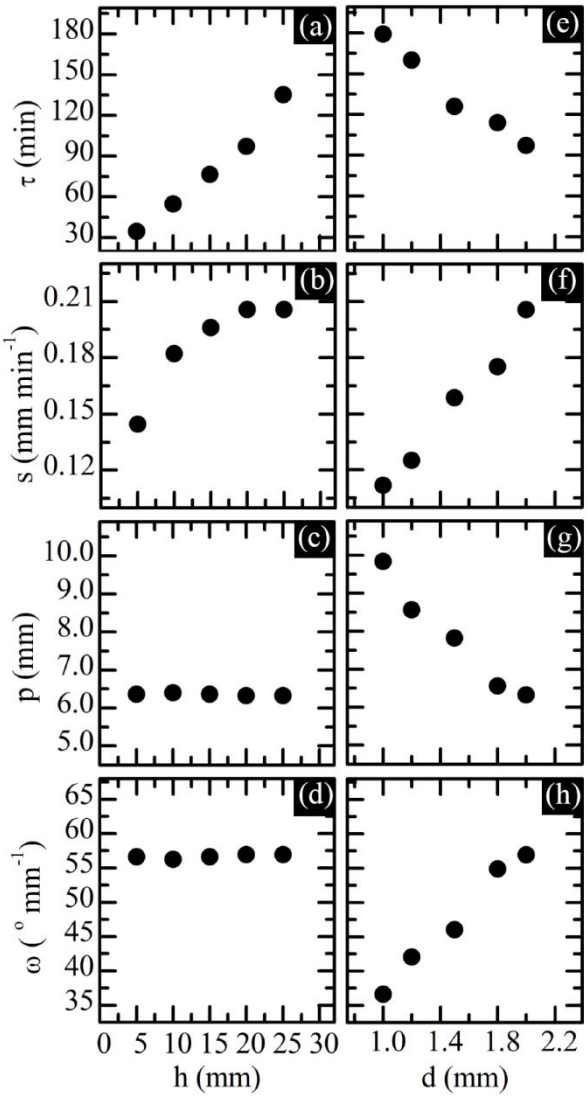

Fig. 4. Analysis of partially pinned scroll waves in the experimental BZ system. (a) The transient time interval τ, (b) the average speed *s* of the downward motion of the twisted structure, (c) the helical pitch *p* and (d) the twist rate ω as functions of the obstacle length *h* for a constant obstacle diameter, *d* = 2.0 mm. (e)-(h) The same quantities as a function of the obstacle diameter *d* for a constant obstacle length, *h* = 20.0 mm.

We analyze the propagation of scroll waves partially pinned to obstacles of different sizes, as shown in Fig. 4. For a given obstacle diameter, $d = 2.0$ mm, the transient time interval τ increases with the obstacle length *h*, Fig. 4(a). A linear fit provides an estimate of the rate $\Delta\tau/\Delta h = 4.5$ min mm^{-1}. During this transition, the twisted structure moves downwards along the obstacle with an

average speed s ($s = \tau/h$) that increases with the obstacle length up to 20.0 mm, beyond which s is approximately constant for larger h, Fig. 4(b). For $h \leq 20.0$ mm, the dependence of s on h is parabolic: $s = 9.8 \times 10^{-2} + 1.1 \times 10^{-2}\, h - 2.8 \times 10^{-4}\, h^2$. Once the twisted structure is completely developed, its pitch $p = 6.3 \pm 0.1$ mm, Fig. 4(c), and its twist rate $\omega = 57.0 \pm 0.6°$ mm^{-1} ($\omega = 360°/p$), Fig. 4(d). Pitch and twist rate are almost independent of the obstacle length h.

In contrast, the obstacle diameter affects the partially pinned scroll wave in a completely different manner. All four variables depend on the obstacle diameter d as approximately linear functions. When d is increased for a given obstacle length, $h = 20.0$ mm, the transient time interval τ decreases with $\Delta\tau/\Delta d = -80.4$ min mm^{-1}, Fig. 4(e), as the downward speed s of the twist increases with $\Delta s/\Delta d = 9.1 \times 10^{-2}$ min^{-1}, Fig. 4(f). The larger the obstacle diameter, the shorter the pitch p of the twisted wave with $\Delta p/\Delta d = -3.5$, Fig. 4(g), but the higher the twist rate ω with $\Delta\omega/\Delta d = 20.6°$ mm^{-2}, Fig. 4(h).

III. SIMULATIONS

A. Simulation Methods

We have carried out simulations of partially pinned scroll waves using the two-variable Oregonator model [37, 38]. The model describes the reaction-diffusion dynamics of the activator u and the controller v corresponding to the concentrations of the autocatalyst $HBrO_2$ and the oxidized form of the metal catalyst (ferriin) in the BZ reaction, respectively:

$$\frac{\partial u}{\partial t} = \frac{1}{\varepsilon}\left(u - u^2 - fv\frac{u-q}{u+q}\right) + D_u \nabla^2 u\,,$$

$$\frac{\partial v}{\partial t} = u - v + D_v \nabla^2 v\,. \qquad (1)$$

Following the study of Jahnke and Winfree [38], the parameters in Eq. (1) are $\varepsilon = 0.01$, $q = 0.002$, $f = 1.4$, with the diffusion coefficients $D_u = 1.0$ and $D_v = 0.6$. In the absence of obstacles, the system supports scroll waves with a cylindrical core of 0.9 dimensionless space units (s.u.) in diameter. The 3D Laplace operator is approximated using a 27-point discretization [40]. The system size is 60×60×80 s.u., with a uniform grid space of 0.2 s.u. and a time step of 0.012 dimensionless time

units (t.u.). No-flux boundary conditions are used for the boundaries of the system and for the obstacle, as described in Ref. [41]. A free scroll wave is initiated by a partition method and allowed to rotate until its shape remains unchanged. A cylindrical obstacle is then inserted at the core of the wave to form a partially pinned scroll wave, as shown in Fig. 5(a). Two series of cylindrical obstacles are used: (1) cylinders with a fixed diameter of 2.0 s.u. and 10.0 – 60.0 s.u. in length, and (2) cylinders with a fixed length of 40.0 s.u. and 1.6 – 10.0 s.u. in diameter.

B. Simulation Results

Figure 5 shows an example of a partially pinned scroll wave from simulations using the Oregonator model. Grayscale images (bottom row) depict lateral projections of the activator u in the whole volume, and the brightness therefore corresponds to the average of u along the projection direction. For enhanced visualization, the isoconcentration surfaces, with $u = 0.4$, in the inner volume are plotted (top row) in light blue with a clear background. The obstacle is placed in the middle of the volume where the filament of a preexisting straight scroll wave is located such that the lower part of the scroll wave is pinned to the obstacle, while the upper part rotates freely, as shown in Fig. 5(a).

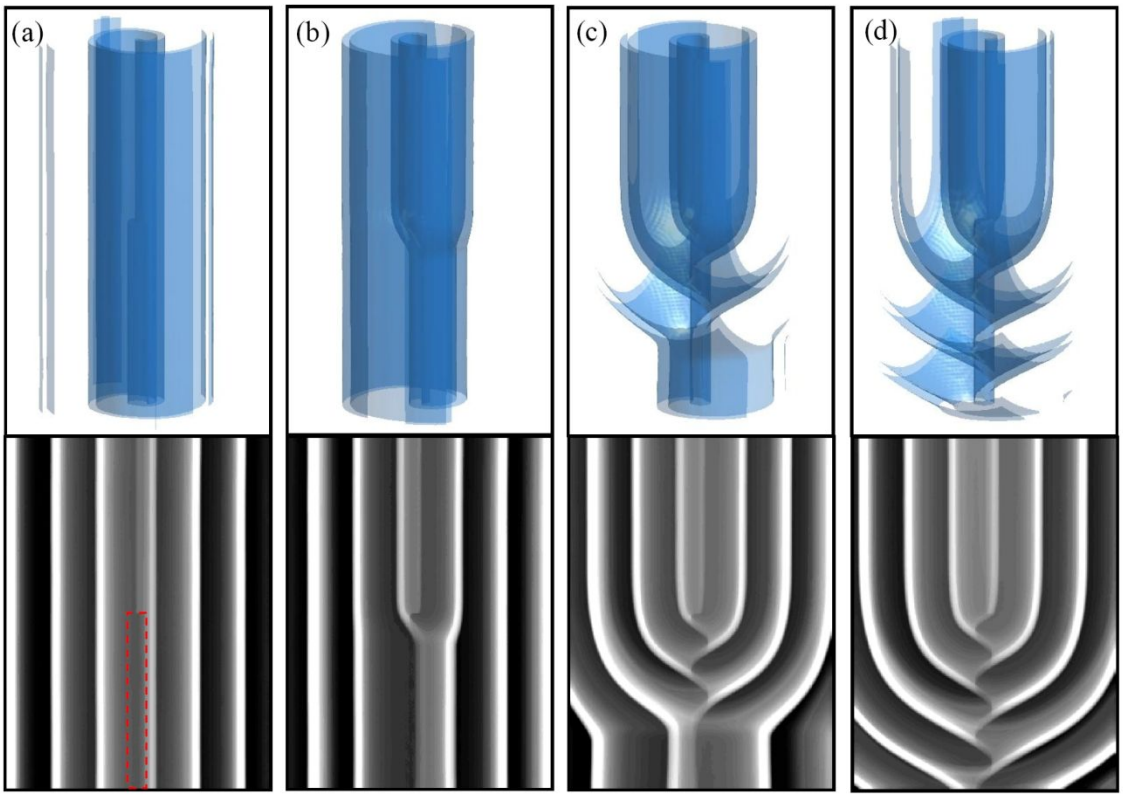

Fig. 5. Images of a partially pinned scroll wave simulated with the Oregonator model. Behavior at (a) 0.0, (b) 2.4, (c) 13.2, and (d) 27.3 t.u. after a cylindrical obstacle, shown by the dashed red rectangle in (a), is inserted into the system. The top and bottom rows depict isoconcentration surface plots of the inner volume and lateral projections of the volume, respectively. The obstacle dimensions are 4.0 s.u. in diameter and 40.0 s.u. in length.

Even though the procedure to generate the pinned wave slightly differs from that in the experiments, the effect of the obstacle can be observed almost immediately after it is placed near the filament, in agreement with the experimental behavior. It can be clearly seen in Fig. 5(b), after the first rotation, that the wave front pinned to the obstacle propagates behind that of the freely rotating scroll wave. Much like the experimental behavior, the interaction of the freely rotating scroll wave with the obstacle gives rise to a pinned twisted scroll wave, where the periods of the two types of waves are equal, as shown in Fig. 5(c). The wave along the lower part of the obstacle is unaffected at this point in time. Finally, the twisted scroll wave, which helically wraps around the obstacle, extends along its entire length, Fig. 5(d), after it completely displaces the original pinned scroll wave.

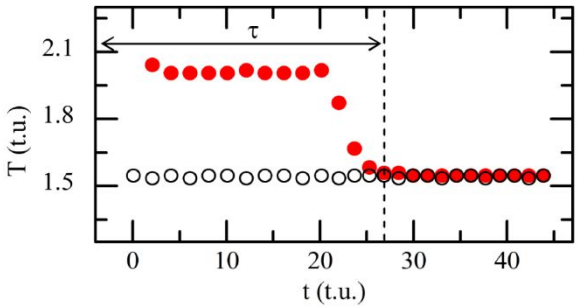

Fig. 6. Wave period T of a partially pinned scroll wave as a function of time in simulations with the Oregonator model. The obstacle dimensions are 4.0 s.u. in diameter and 40.0 s.u. in length. Open (white) and filled (red) circles represent the periods of the freely rotating scroll wave in the upper region and the pinned scroll wave in the lower region, respectively. The periods of the freely rotating scroll waves and the pinned scroll waves become equal to each other after the pinned twisted scroll wave replaces the original pinned scroll wave following the transient time interval τ.

In order to observe the effects of the obstacles on the scroll waves, the wave periods are measured at locations near the center of the upper and the lower cross sections, with the later close to the obstacle. An example of such measurements is shown in Fig. 6. The freely rotating scroll wave in the upper region has a constant period of 1.55 t.u. The obstacle immediately affects the pinned scroll wave in the lower region after it is placed along the wave filament; the wave period T of the pinned wave slightly overshoots, changing from 1.55 t.u. to 2.04 t.u. within the first rotation. For 0 t.u. $\leq t \leq$ 20.2 t.u., in which the twisted wave structure is developing along the obstacle, the period T in the lower region is almost constant with a period of 2.02 t.u. As the twisted scroll wave approaches the bottom of the obstacle, replacing the original pinned scroll wave, T decreases to 1.55 t.u. within 4 wave rotations in the time interval 20.2 t.u. $< t <$ 26.8 t.u. Finally, the entire scroll wave, made up of freely rotating and pinned and twisted parts, has the same period of 1.55 t.u.

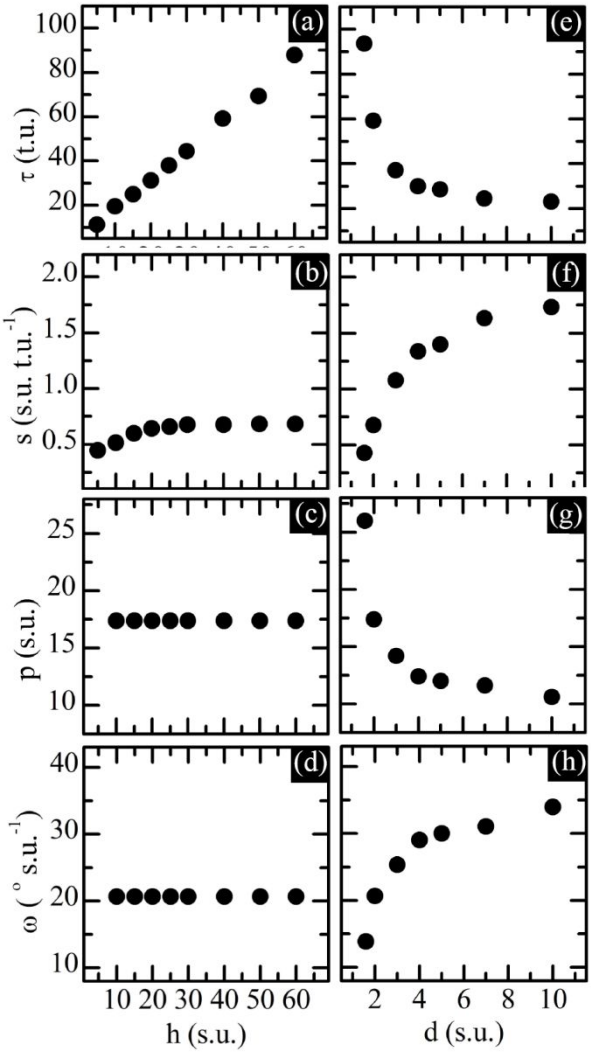

Fig. 7. Analysis of partially pinned scroll waves in simulations with the Oregonator model. (a) The transient interval τ, (b) the average speed *s* of the downward motion of the twisted structure, (c) the helical pitch *p* and (d) the twist rate ω as a function of the obstacle length *h*, for a constant obstacle diameter, $d = 2.0$ s.u. (e)-(h) The same quantities as a function of the obstacle diameter *d*, for a constant obstacle length, $h = 20.0$ s.u.

An analysis of the scroll wave dynamics from the simulations is summarized in Fig. 7. For a given obstacle diameter $d = 2.0$ s.u., the transient time interval τ increases linearly with the obstacle length *h* with a rate $\Delta\tau/\Delta h = 1.35$ t.u. s.u.$^{-1}$, Fig. 7(a). The average speed *s* of the twisted structure moving downward during this transition slightly increases for $h \leq 30.0$ s.u. but is almost constant for longer obstacles, Fig. 7(b). For $h \leq 30.0$ mm, s depends on *h* as a parabolic function:

$s = 0.34 + 2.24 \times 10^{-2} h - 3.76 \times 10^{-4} h^2$. After the twist is fully developed, its pitch $p = 17.40$ s.u., Fig. 7(c), and twist rate $\omega = 20.69°$ s.u.$^{-1}$, Fig. 7(d), are independent of the obstacle length h.

For a given obstacle length, $h = 20.0$ s.u., an increment of the obstacle diameter d results in a reduction of the transient time interval τ, Fig. 7(e), and an increase in the downward moving speed s of the twist, Fig. 7(f). The larger the obstacle diameter, the shorter the pitch p of the twisted wave, Fig. 7(g), but the higher the twist rate ω, Fig. 7(h). These simulation results are qualitatively similar to those in the experiments (Figs. 4(e) – 4(h). However, the curves shown in Figs. 7(e) – 7(h) can be fit well with exponential functions: $\tau = 25.87 + 7.31 \times 10^2 \exp(-1.50d)$, $s = 1.74 – 2.68 \exp(-0.45d)$, $p = 11.85 + 3.26 \times 10^2 \exp(-1.97d)$, and $\omega = 32.58 – 51.23 \exp(-0.67d)$, while the experimental results in Figs. 4(e) – 4(h) show an approximately linear dependence on d. This discrepancy may be due to the difference in the range of obstacle size used in the experiments and the simulations. In the experiments, the obstacle diameter d ranges from about 1 to 2 times the spiral core diameter ($d_s \sim 1$ mm [41]), while d ranges from about 1.6 to 10 times the spiral core diameter ($d_s \sim 1$ s.u. [41]) in the simulations.

IV. DISCUSSION

We have presented an investigation of the dynamics of scroll waves partially pinned to unexcitable cylindrical obstacles of different lengths and diameters in 3D Belousov-Zhabotinsky excitable media. Our experimental findings and results of our numerical simulations with the Oregonator model are in excellent qualitative agreement. The obstacles affect the wave propagation almost immediately after the partially pinned scroll waves are created in the experiments, where the scroll wave is initiated around a previous placed obstacle, and in the simulations, where an obstacle is placed along the filament of a preexisting free scroll wave. In both the experiments and simulations, a longer period of the pinned scroll wave compared to the period of the freely rotating scroll wave is quickly observed.

In the absence of obstacles, twisted scroll waves have been created in the BZ reaction subjected to gradients in temperature [16, 17], oxygen concentration [18] or CO_2 concentration [19, 20]. Because these gradients, as well as wave period, are smooth functions of position, the twisted wave occurs along the entire filament. In contrast, the partially pinned scroll waves in this study are twisted only in the pinned region, while the freely rotating scroll wave remains

unaffected. Initially, the period of the pinned scroll wave, which is longer than that of the freely rotating wave, is equal along the obstacle. However, as the faster freely rotating scroll wave begins to interact with the obstacle, it forms a faster twisted scroll wave that begins to displace the slower pinned wave. As the pinned twisted wave becomes fully developed, replacing the slower pinned wave, the scroll wave helically wraps around the entire obstacle, with the period of the twisted scroll wave equal to the period of the freely rotating scroll wave. As the obstacle diameter is increased, the twist rate increases and the helical pitch decreases; however, the period of the twisted scroll wave is always equal to the freely rotating scroll wave.

ACKNOWLEDGEMENTS

We thank the Research and Development Institute (KURDI), the Center for Advanced Studies of Industrial Technology, the Graduate School, the Capacity Building on Academic Competency of KU Students, Kasetsart University, the Thailand Research Fund (Grant No. RSA5880033) and the Office of the Higher Education Commission and King Mongkut's University of Technology North Bangkok (Grant No. KMUTNB-GOV-59-19) for financial support. K.S. is grateful to the National Science Foundation (USA) for financial support with Grant No. CHE-1565665.

REFERENCES

[1] A. T. Winfree, *Science*, 1972, **175**, 634.
[2] A. T. Winfree, *Science*, 1973, **181**, 937.
[3] J. J. Tyson and S.H. Strogatz, *Int. J. Bif. Chaos*, 1991, **1**, 723.
[4] A. T. Winfree, *Science*, 1994, **266**, 1003.
[5] R.A. Gray, A.M. Pertsov, and J. Jalife, *Nature* (*London*), 1998, **392**, 75.
[6] F. Fenton, E.M. Cherry, H M. Hastings, and S.J. Evans, *Chaos*, 2002, **12**, 852.
[7] V.N. Biktashev, A.V. Holden, and H. Zhang, *Phil. Trans. R. Soc. Lond. A*, 1994, **347**, 611.
[8] H. Henry and V. Hakim, *Phys. Rev. E*, 2002, **65**, 046235.
[9] S. Alonso, F. Sagues, and A.S. Mikhailov, *Science*, 2003, **299**, 1722.
[10] T. Bansagi and O. Steinbock, *Phys. Rev. E*, 2007, **76**, 045202(R).

[11] C. Luengviriya, U. Storb, G. Lindner, S.C. Müller, M. Bär, and M.J.B. Hauser, *Phys. Rev. Lett.*, 2008, **100**, 148302.

[12] A. Rusakov, A.B. Medvinsky, and A.V. Panfilov, *Phys. Rev. E*, 2005, **72**, 022902.

[13] D. Kupitz and M. J. B. Hauser, *Phys. Rev. E*, 2012, **86**, 066208.

[14] C. Henze, E. Lugosi, and A.T. Winfree, *Can. J. Phys*., 1990, **68**, 683.

[15] I. Aranson and I. Mitkov, *Phys. Rev. E*, 1998, **54**, 4556.

[16] A.M. Pertsov, R.R. Aliev, and V.I. Krinsky, *Nature*, 1990, **345**, 419.

[17] S. Mironov, M. Vinson, S. Mulvey, and A.M. Pertsov, *J. Phys. Chem.*, 1996, **100**, 1975.

[18] U. Storb, C.R. Neto, M. Bär, and S.C. Müller, *Phys. Chem. Chem. Phys.*, 2003, **5**, 2344.

[19] D. Kupitz, S. Alonso, M. Bär, and M. J. B. Hauser, *Phys. Rev. E*, 2011, **84**, 056210.

[20] P. Dähmlow, S. Alonso, M. Bär, and M. J. B. Hauser, *Phys. Rev. Lett*., 2013, **110**, 234102.

[21] J. M. Davidenko, A. M. Pertsov, R. Salomonz, W. Baxter, and J. Jalife, *Nature*, 1992, **335**, 349.

[22] J. P. Keener and J. J. Tyson, *Physica D*, 1986, **21**, 307.

[23] Y.-Q. Fu, H. Zhang, Z. Cao, B. Zheng, and G. Hu, *Phys. Rev. E*, 2005, **72**, 046206.

[24] Z. Y. Lim, B. Maskara, F. Aguel, R. Emokpae, and L. Tung, *Circulation*., 2006, **114**, 2113.

[25] C. Cherubini, S. Filippi, and A. Gizzi. *Phys. Rev. E*, 2012, **85**:031915,

[26] M. Sutthiopad, J. Luengviriya, P. Porjai, M. Phantu, J. Kanchanawarin, S.C. Müller, and C. Luengviriya, *Phys. Rev. E*, 2015, **91**, 052912.

[27] M. Tanaka, A. Isomura, M. Hörning, H. Kitahata, K. Agladze, and K.Yoshikawa, *Chaos*, 2009, **19**, 043114.

[28] M. Tanaka, M. Hörning, H. Kitahata, and K. Yoshikawa, *Chaos*, 2015, **25**, 103127.

[29] M. Sutthiopad, J. Luengviriya, P. Porjai, B. Tomapatanaget S. C. Müller, and C. Luengviriya, *Phys. Rev. E*, 2014, **89**, 052902.

[30] P. Porjai, M. Sutthiopad, J. Luengviriya, M. Phantu, S.C. Müller, C. Luengviriya, *Chem. Phys. Lett*., 2016, **660**, 283.

[31] Z. Jiménez, B. Marts and O. Steinbock, *Phys. Rev. Lett*., 2009, **102**, 244101.

[32] Z. Jiménez and O. Steinbock, *Europhys. Lett*., 2010, **91**, 50002.

[33] Z.A. Jiménez and O. Steinbock, *Phys. Rev. E*, 2012, **86**, 036205.

[34] H. Ke, Z. Zhang, and O. Steinbock, *Phys. Rev. E*, 2015, **91**, 032930.

[35] S. Sridhar1, A. Ghosh, and S. Sinha, *EPL.*, 2013**, 103**, 50003.

[36] F. Spreckelsen, D. Hornung, O. Steinbock, U. Parlitz, and S. Luther, *Phys. Rev. E*, 2015, **92**, 042920.

[37] R. J. Field and R. M. Noyes, *J. Chem. Phys*., 1974, **60**, 1877.

[38] W. Jahnke and A. T. Winfree, *Int. J. Bif. Chaos*, 1991, **1**, 445.

[39] C. Luengviriya, U. Storb, M. J. B. Hauser, and S. C. Müller, *Phys. Chem. Chem. Phys*., 2006, **8**, 1425.

[40] M. Dowle, R. M. Mantel, and D. Barkley, *Int. J. Bif. Chaos*, 1997, **7**, 2529.

[41] J. Luengviriya, M. Sutthiopad, M. Phantu, P. Porjai, J. Kanchanawarin, S. C. Müller, and C. Luengviriya. *Phys. Rev. E*, 2014, **90**, 052919.